Journal of Hazardous Materials 474 (2024) 134657

Contents lists available at ScienceDirect

Journal of Hazardous Materials

journal homepage: www.elsevier.com/locate/jhazmat

Hazardous element inertisation in vitrified silicate ceramics: Effect of different matrices

S. Conte [a,*], C. Molinari [a], M. Ardit [b], L. Mantovani [c], M. Tribaudino [d], G. Cruciani [b], M. Dondi [a], C. Zanelli [a]

[a] CNR–ISSMC, Institute of Science, Technology and Sustainability for Ceramics, Via Granarolo 64, 48018 Faenza, Italy
[b] Physics and Earth Sciences Department, University of Ferrara, Via Saragat 1, 44122 Ferrara, Italy
[c] Department of Chemical, Life and Environmental Sustainability Sciences, University of Parma, Parco Area delle Scienze 11/a, 43124 Parma, Italy
[d] Earth Sciences Department, University of Turin, Via Verdi 8, 10124 Turin, Italy

HIGHLIGHTS

- Circular economy in ceramic industry: effective recycling of various industrial waste.
- Quantitative evaluation of immobilisation efficiency for 11 hazardous elements.
- Vitrified ceramics: high immobilisation efficiency, depending on composition.
- Poor retention of Mo in ceramic bodies, related to oxyanionic complexes.

GRAPHICAL ABSTRACT

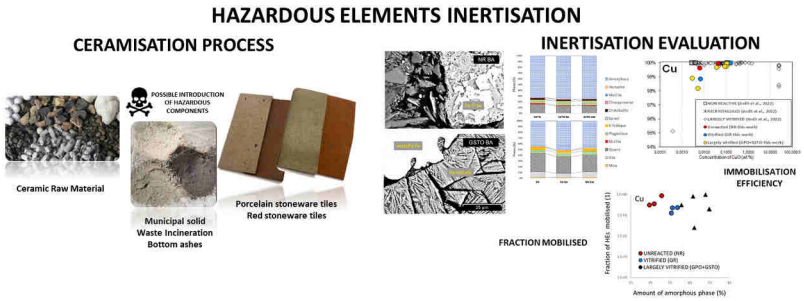

ARTICLE INFO

Keywords:
Red stoneware
Porcelain stoneware
Element mobility
Immobilisation efficiency
Ceramisation process

ABSTRACT

The ceramic industry is a production sector that can efficiently recycle its own processing residues, achieving a reuse index of almost 100%. Recently, the range of waste from other industrial sectors that can be used as secondary raw materials in ceramic bodies has expanded. However, such an expansion potentially introduces hazardous components. This study aimed to quantitatively assess the efficiency of inertising hazardous elements (HEs) through ceramisation. The ceramics were characterised through XRPD, SEM-EDS and leaching tests to determine their leaching behaviour and the mechanisms of element immobilisation in neoformation phases during the ceramisation process. The results indicate high immobilisation efficiency for Ba, Co, Cr, Cu, Pb, Sb, Sn and Zn. However, Mo is the main element of concern owing to its poor retention in ceramic bodies. This is likely due to the formation of oxyanionic complexes that are difficult to immobilise in silicate matrices. In addition, the ceramic bodies exhibit substantial differences that appear to be associated with variations in pseudo-structural components and the degree of polymerisation of their vitreous phase.

* Correspondence to: CNR–ISSMC, Via Granarolo 64, 48018 Faenza, Italy.
E-mail address: sonia.conte@issmc.cnr.it (S. Conte).

https://doi.org/10.1016/j.jhazmat.2024.134657
Received 16 January 2024; Received in revised form 13 May 2024; Accepted 17 May 2024
Available online 20 May 2024

1. Introduction

In recent years, there has been increasing pressure to accelerate the transition to circular economy, particularly in established sectors such as ceramics, where waste recycling is the most feasible option [1-3]. However, ceramic production is also a valuable option for mineral waste valorisation. The large volumes of raw materials used and the high-temperature treatment involved in the process can effectively stabilise the waste in the ceramic matrix [4,5]. Nevertheless, these heat treatments can also induce phase transformations that may affect the efficiency of stabilisation of certain elements [6,7].

The substitution of natural raw materials with mineral waste may introduce elements, some of which are potentially hazardous, that are only present in trace amounts in conventional formulations. This can be a conscious choice, as in the case of screen and cathode-ray tube recycled glasses containing Ba, Sr and Pb [8-10] or sludge from galvanising/plating plants containing Cr, Ni and Zn [11-13]. In some cases, unintentional additions occur due to contamination by heavy metals, such as in the case of dredged harbour sediments [14-16] or spent foundry sands [11,17,18].

The effectiveness of inertising hazardous elements (HEs) depends on the ceramic matrix in which the waste is added, in addition to the process conditions [4,6,7]. There are two categories of ceramic bodies with different stabilisation mechanisms: largely vitrified and largely recrystallised bodies. The former category results in dense products with negligible porosity, whereas the latter category results in less dense and more porous products. Within the vitrified product category, the most important types are *porcelain stoneware* and *red stoneware*, which alone account for a large portion of the global production of ceramic tiles [19, 20]. Porcelain stoneware and red stoneware have an estimated annual production of about 200 million tons per year, making them an important potential source for mineral waste recycling [21-24].

Research on HEs stabilisation has mainly focused on recrystallised and porous products, such as those used in the production of clay bricks and wall tiles [25-28]. Only a few studies have addressed largely vitrified ceramic bodies. These case studies examine the recycling of specific waste types, such as recycled glass [8,9,29,30,31], metallurgical slags [32-34], heavy metal–rich sludges [13,35,36], waste from titania production [37] and Municipal Solid Waste Incineration (MSWI) ashes [32, 38-44]. MSWI ashes are a special case owing to their high levels of chlorine and sulfur [45,46], which can considerably disrupt the stabilisation process of heavy metals [47–53].

Another area of research focuses on the development of glass ceramics that contain a substantial amount of waste material while also controlling the leaching behaviour of HEs ([5,54-57], among many others). However, the compositions and thermal processes required for this approach differ from those used in industrial ceramics. The goal is to first achieve a molten state and then a controlled crystallisation, obtaining highly crystallised products. For these reasons, these contributions are not directly useful for our purposes.

Although many studies have been conducted to understand the leaching behaviour of HEs in silicate matrices (e.g. [6,46,51,53,58]), there is no comprehensive evaluation specifically on aluminosilicate vitreous compounds, such as those found in widely vitrified ceramic products. Silicate ceramics are generally effective in immobilising Ba, Cd, Ni and Zn but may not be sufficient for Mo, As and Cr, presumably due to oxy-anionic complexes, and for Pb and Cu. The leaching behaviour of aluminosilicate glasses can be greatly influenced by differences in their chemical composition and structure [59-63]. Therefore, the release of HEs introduced with a given waste in porcelain stoneware or in red stoneware may be different, with dissolution kinetics that may vary depending on the vitreous matrices' pseudo-structural components and degree of polymerisation. However, the literature on leaching of HEs from ceramic matrices does not provide information on glass composition.

The sustainability of the ceramic industry heavily relies on its capacity to enhance resource efficiency and transition to a circular economy. These objectives are achieved in ceramic production by increasing waste recycling. The main challenge is controlling the fate of HEs that may be present in waste materials. This study aimed to investigate the leaching behaviour of HEs contained in vitrified bodies, namely, red stoneware and porcelain stoneware, which are the most popular materials in tile-making. Furthermore, the glassy phase is believed to have the most interaction with the phases containing HEs, making it crucial for their stabilisation. The HEs considered in this study were Ba, Co, Cr, Cu, Mo, Pb, Sb, Sn, Sr, V and Zn. These elements may be found in residues that are used (or potential candidates) as secondary raw materials in ceramic tiles.

For the purpose of comparison, we also studied the equivalent of red stoneware with a largely amorphous matrix. This represents the case of ceramic products fired at relatively low temperatures to yield porous products with low carbon footprints. In addition, we investigated the effect of inorganic compounds, namely, Cl and S, which are volatilised during firing and added in the form of untreated MSWI bottom ash (BA), on the stabilisation of heavy metals.

2. Experimental

Four batches were designed according to the industrial recipes to obtain one vitrified and two largely vitrified ceramic products (i.e. a red stoneware and two different porcelain stoneware bodies) and one largely unreacted body (low-fired brick). Specifically, the two porcelain stoneware batches are represented by a classic body (GPO) and a 'glass-ceramic stoneware' (GSTO), taking into account new batches designed under the circular economy concept recycling glass cullet [9,29,30, 64–76]. GPO and GSTO were formulated with the same raw materials, i.e. ball clay, kaolin, sodic feldspar and quartz sand, in different proportions. Furthermore, a silica–lime–soda glass (SLS), currently used in tile-making, was utilised in the GSTO formulation. The red stoneware (GR) and the low-fired brick (NR) were made at 100% with the same red clay (Table 1 for batch formulation and Table S1, supplementary material, for the chemical–mineralogical composition of raw materials). The different firing schedules, between GR and NR, enabled the yield of distinct finished products.

The chemical composition of the raw batches was determined through X-ray fluorescence by wavelength-dispersive spectrometry (XRF-WDS, Axios-Panalytical; 4-kW Rh tube). The main components are reported in Table 1, whereas both major and minor oxides are given in Table S2 as supplementary information. The accuracy of determination was better than 3% relative, whereas the precision for major constituents was between 1% and 2% (relative) and that for the minor constituents was in the range of 2–3% (threes replicates). The four reference

Table 1
Formulation and chemical composition of the raw batches.

	Unit	GPO	GSTO	GR	NR
Ball clay	wt%	30	40	-	-
Kaolin	wt%	5	-	-	-
Red clay	wt%	-	-	100	100
Quartz sand	wt%	15	13	-	-
Sodic feldspar	wt%	50	27	-	-
Soda lime glass	wt%	-	20	-	-
SiO_2	wt%	70.62	70.15	62.44	62.44
TiO_2	wt%	0.66	0.73	0.80	0.80
Al_2O_3	wt%	17.69	15.02	16.16	16.16
Fe_2O_3	wt%	1.20	0.99	6.68	6.68
MgO	wt%	0.52	0.79	2.38	2.38
CaO	wt%	0.75	2.68	1.32	1.32
MnO	wt%	0.02	0.02	0.17	0.17
Na_2O	wt%	3.28	4.31	1.45	1.45
K_2O	wt%	1.41	1.39	2.70	2.70
P_2O_5	wt%	0.23	0.20	0.12	0.12
Loss on ignition, LoI	wt%	3.63	3.73	5.77	5.77

bodies were tested at the laboratory scale. For the porcelain stoneware batches GPO and GSTO, a wet grinding process was adopted: all raw materials were ball-milled in a porcelain jar using dense alumina balls as grinding media, 40% water (by weight of the slip) and 0.3% deflocculant (sodium tripolyphosphate, by weight of dry batch) for 15 min. The slips were oven-dried and then de-agglomerated (1-mm mesh hammer mill). Unlike the previous samples, the red clay batches (GR and NR) were dry-de-agglomerated in a porcelain mortar until all the powder passed through a 500-μm sieve. Upon obtaining the reference batches, an artificial laboratory waste was designed to have a single material containing the HEs considered in this study to simplify batch preparation. This material is not intended to simulate a specific type of waste but to constitute a case study with various HEs occurring simultaneously, as often occurs with residues added to ceramic materials. The concentrations of HEs were selected high enough to make the determination of eluates robust, taking into account the degree of dilution of artificial waste (AW) in the ceramic body and the usual concentrations of eluates from ceramic materials. Starting from a ceramic sludge and a Si–Na glass used as matrix, the following reagents were added: $BaCO_3$, Co_3O_4, Cr_2O_3, CuO, MoO_3, Sb_2O_3, SnO_2, $SrCO_3$, V_2O_5, ZnO and PbO. Sludge and glass were selected because they have a composition comparable with that of the ceramic matrices where the AW would be inserted and because the sludge already contains ZnO. The sludge and the reagents already had a fine particle size (<100 μm), whereas the glass, before being added, was wet-milled for 10 min in a porcelain jar using dense alumina balls as grinding media (Magellano, Ceramics Instruments) and then oven-dried. The obtained mixture (containing ceramic sludge, glass and reagents) was homogenised by mixing it in a polyethylene bottle for 2 h in a turbula, yielding the so-called AW. Simultaneously, a real waste-containing HEs (Cr, Cu, Zn, Pb) was also taken into consideration to explore the effect of Cl and S, present in relatively high amounts, on the inertisation of HEs. Specifically, the bottom fraction of the MSWI ash coming from the Ferrara (Italy) incinerator was chosen. This bottom ash (BA) was dry-ground using a hammer mill with a 200-μm mesh to avoid reactions in contact with water. The chemical compositions of the AW and BA were determined through XRF-WDS and are listed in Table 2. At this point, the AW and BA were separately added to the starting batches. The powders of the reference bodies were divided into three lots to obtain a waste-free body (without addition), a body with addition of 10 wt% BA and another one with 10 wt% of AW. By this way, 12 batches were obtained (four reference bodies × three formulations), labelled with the acronyms of the waste, e.g. series GPO/GPO-BA/GPO-AW. The 12 mixtures were homogenised by mixing them in a polyethylene bottle for 1 h in a three-dimensional mixer (Turbula). Then, they were humidified (5 wt% of water for red clay batches and 8 wt% for porcelain stoneware) and manually granulated (1-mm sieve). The powders were compacted with a hydraulic press (40 MPa) into 110 × 55 × 5 mm tiles, oven-dried in an electric oven at 105 °C ± 5 °C overnight and characterised for springback (i.e. 100(*L*p − *L*m)/*L*m, where *L*p denotes the length of the pressed tile and *L*m is the length of the mould) and green and dry bulk density (weight/volume ratio) (Table 3). Porcelain stoneware and red stoneware powder compacts were fast-fired (60-min cold-to-cold cycle) in an electric chamber kiln (Nannetti, Italy) at different maximum temperatures (T_{max}): 1210 °C, 1220 °C and 1120 °C for the GPO, GSTO and GR series, respectively. Otherwise, the unreacted body series (NR/NR-BA/NR-AW) was slow-fired in an electric aspirated kiln (Nannetti KL40/12 S) at 820 °C for 12 h.

Table 2
Chemical composition of the artificial waste and MSWI bottom ash.

wt%	Artificial waste			Bottom ash		
SiO_2	49.07	±	0.74	33.39	±	0.50
TiO_2	0.51	±	0.02	0.88	±	0.03
ZrO_2	2.36	±	0.07	0.02	±	0.00
SnO_2	1.56	±	0.05	0.01	±	0.00
Al_2O_3	14.84	±	0.22	8.82	±	0.13
Cr_2O_3	1.25	±	0.04	0.11	±	0.00
Fe_2O_3	1.13	±	0.02	7.72	±	0.12
Sb_2O_3	1.36	±	0.04	0.00	±	0.00
MgO	0.88	±	0.03	2.92	±	0.09
CaO	5.96	±	0.11	31.75	±	0.57
MnO	0.87	±	0.03	0.20	±	0.01
CoO	1.06	±	0.03	0.00	±	0.00
CuO	0.92	±	0.03	0.28	±	0.01
ZnO	3.38	±	0.10	0.44	±	0.01
SrO	0.88	±	0.03	0.00	±	0.00
BaO	1.71	±	0.05	0.13	±	0.00
PbO	1.10	±	0.03	0.37	±	0.01
Na_2O	2.54	±	0.05	2.57	±	0.05
K_2O	2.32	±	0.04	1.11	±	0.02
V_2O_5	1.37	±	0.04	0.01	±	0.00
MoO_3	0.99	±	0.03	0.00	±	0.00
Cl	0.19	±	0.01	1.31	±	0.04
S	0.14	±	0.00	1.27	±	0.04
LoI	3.60			6.70		

The technological properties determined after firing the samples at different T_{max} were (Table 3): linear firing shrinkage (i.e. 100(*Lm–Lf*)/*Lm* where *Lf* denotes the length of the fired tiles and *Lm* denotes the length of the mould), water absorption and bulk density (ASTM C373). The chemical compositions are listed in Table S2, supplementary materials

The phase composition of the fired products was quantitatively assessed through X-ray powder diffraction (XRPD). Data collection was performed at room temperature using a Bruker D8 Advance Da Vinci diffractometer (available at the Physics and Earth Sciences Dept., University of Ferrara) operating in Bragg–Brentano geometry and equipped with a Cu-anode X-ray tube, Ni-filter to suppress the Cu–*Kβ* component and a LynxEye XE silicon strip detector (2.585° of window size) set to discriminate the Cu–$K\alpha_{1,2}$ radiation. Each sample powder was scanned in a continuous mode in the 5–90° 2θ angular range with a step size of 0.02° 2θ and a counting time of 2 s per step. A knife perpendicular to the sample was placed at a suitable distance from the sample surface to reduce air-induced scattering. Before the XRPD measurements, each sample was mixed with 20 wt% corundum (NIST alumina powder SRM 676) as an internal standard for the quantification of the crystalline phases and XRD amorphous content and then ground using an agate mortar and pestle [77,78]. Qualitative phase analysis was conducted using the EVA software version 6 (Bruker). The collected XRPD patterns were modelled using the fundamental parameter Rietveld approach (TOPAS v.5, Bruker). Because the certified weight percentage of crystalline corundum SRM 676 was 91.75(± 1.52) wt%, the weight fraction of the crystalline corundum used as an internal standard to obtain the correct value of the amorphous fraction of the investigated samples was maintained at 18.35 wt% during the refining procedure (i.e. the corundum was treated as a spiked phase with a crystalline phase fraction of 20 wt% * 0.9175 = 18.35 wt%). All the identified phases were modelled by performing multi-phase refinements. Known instrumental parameters (e.g. goniometer radius, slit sizes, X-ray tube geometric parameters) were used to calculate the instrumental contribution to the peak profiles, the zero-error correction was fixed at the value determined using the NIST Si standard (SRM 640e), and refinements included a sample displacement correction and a Chebyshev polynomial curve to model the background. The Rietveld refinement plot of some of the collected XRPD patterns is reported as a supplementary material (Fig. S1).

To study the microstructure of the fired bodies, samples of approximately 0.5 * 0.5 cm were cut and embedded in resin, polished and then examined using a Jeol 6400 scanning electron microscope equipped with an Oxford energy-dispersive spectrometer (SEM-EDS). EDS investigation of specific areas of interest was conducted to gain better understanding of element diffusion. The analytical conditions were 20-kV and 1.2-mA current, ~1-mm beam diameter and 60-s counting time; several analytical points and chemical maps per sample were performed. Images were obtained using both back-scattered and secondary electron detectors.

Table 3
Technological properties of unfired and fired products: unfired = springback (SPBK), green bulk density (GBD), dry bulk density (DBD); fired = firing temperature (Firing T), firing shrinkage (FS), bulk density (BD), water absorption (WA), *warped.

Tile commercial classification ISO13006	Property		Unfired			Fired			
			SPBK	GBD	DBD	Firing T	FS	BD	WA
	unit		cm/m	g/cm^3	g/cm^3	°C	cm/m	g/cm^3	%
Large vitrified	**GPO**	mean	0.47	2.107	1.959	1210	5.8	2.425	0.39
Group BIa		±	0.01	0.016	0.014		0.3	0.029	0.05
	GPO-BA	mean	0.48	2.090	1.956	1210	5.3	2.330	0.36
		±	0.02	0.013	0.007		0.2	0.002	0.13
	GPO-AW	mean	0.50	2.088	1.941	1210	6.0	2.376	0.15
		±	0.01	0.012	0.009		0.2	0.020	0.09
	GSTO	mean	0.45	2.065	1.914	1220	4.5 *	2.280	0.11
		±	0.01	0.068	0.073		0.3	0.016	0.09
	GSTO-BA	mean	0.46	2.092	1.970	1220	2.6 *	2.189	0.12
		±	0.02	0.006	0.004		0.4	0.007	0.05
	GSTO-AW	mean	0.47	2.088	1.950	1220	2.1 *	2.079	0.09
		±	0.01	0.008	0.022		0.3	0.014	0.01
Semi-vitrified	**GR**	mean	0.48	2.135	2.062	1120	4.0	2.247	6.22
Group BIIb		±	0.02	0.023	0.010		0.3	0.009	0.19
	GR-BA	mean	0.47	2.133	2.082	1120	2.5	2.151	8.06
		±	0.01	0.007	0.067		0.2	0.003	0.12
	GR-AW	mean	0.49	2.135	2.054	1120	4.4	2.237	6.60
		±	0.01	0.006	0.008		0.6	0.003	0.10
Porous	**NR**	mean	0.50	2.140	2.057	820	− 0.4	1.967	13.33
Group BIII		±	0.02	0.013	0.014		0.1	0.015	0.34
	NR-BA	mean	0.48	2.136	2.061	820	− 0.3	1.962	13.66
		±	0.01	0.010	0.007		0.1	0.025	0.74
	NR-AW	mean	0.47	2.138	2.059	820	− 0.3	1.967	13.52
		±	0.01	0.011	0.012		0.1	0.022	0.55

Leaching tests were conducted on all the fired samples to evaluate the mobility of the HEs with a liquid/solid ratio of 10 and a particle size < 4 mm, as required by the EN 12457–2:2002 standard, in both water (pH ranging from 8 to 11) and acetic acid 5% w/w (pH 5). The samples were manually crushed and sieved to achieve a grain size lower than 4 mm. To better discriminate the material properties, the obtained fragments were sieved at 2 mm showing different fractions between 2 and 4 mm (fraction higher than 2 mm: GPO–GSTO~80%; GR~50%; NR~40%). A fraction representative of the whole samples (sieved at 4 mm) was kept in rotation for 24 h, after which the eluate was filtered at 40 μm and analysed using an Agilent 5100 inductively coupled plasma equipped with an optical emission spectrometer (ICP-OES, analysis details in Table S3 supplementary materials) without dilution.

Data elaboration was performed to contrast the leaching data with the total amount of every HE present in the ceramic body. The *fraction mobilised* (f_{HE}) denotes the fraction of HEs that can be released to the total HE amount ($f_{HE} = \xi_{leached}/\xi_{total}$, where $\xi_{leached}$ and ξ_{total} are the relative HE weight fractions in the leachate and ceramic bulk, respectively). Another parameter used to quantify the degree of retention of toxic elements in silicate ceramics is the *efficiency of immobilisation* (ε_{HE}). It expresses the percentage of a given HE that is not mobilised during the leaching test of the waste-bearing ceramic bulk, calculated as $\varepsilon_{HE} = (\xi_{total} - \xi_{leached})/\xi_{total} * 100$. The $\xi_{leached}$ values are calculated from the measured HE concentrations in the leachate solution and then normalised with respect to the extraction volume determined by a specific procedure. The *hazard quotient* (HQ_{HE}) is calculated as $HQ_{HE} = \xi_{leached}/\xi_{limit}$. This parameter shows how close the released HE amount ($\xi_{leached}$) is to the regulatory limit established for inert materials, EU (Dir. 1999/31/EC). HQ_{HE} values above unity indicate that the permissible limit is exceeded.

3. Results and discussion

3.1. Ceramic matrix: phase composition of the ceramic bodies

Fig. 1 shows the phase composition of the 12 samples obtained after firing (see also Table S4 in supplementary material). GPO exhibits the classical porcelain stoneware phase composition, consisting of a low content of feldspar remnants (plagioclase and K-feldspar), residual quartz and neoformation mullite, embedded in an abundant amorphous phase [79].

The porcelain stoneware GSTO, which contains 20 wt% of SLS waste glass in the starting formulation, has a lower amount of quartz and mullite and a higher percentage of plagioclase than GPO. This is due to the peralkaline chemistry of the GSTO body (Fig. 2), related to the presence of glass rich in Ca and Na. This chemistry enhances the stability of feldspars at the expense of mullite formation and quartz persistence, as observed in the literature [80-83]. Both GPO and GSTO have residual plagioclase. In addition, it can be inferred that neoformation plagioclase is present in GSTO. Both batches used the same starting albitite as flux. To determine if the plagioclase in the fired tiles is residual or neoformation, the crystallo-chemical relationships described by Morrison et al. [84] can be applied. According to the refined unit-cell parameters (Equations 1a and 1b [84]), the plagioclase phase in GPO maintains an albitic stoichiometry after firing, whereas the plagioclase phase in GSTO, with a Ca/Na ratio of ~2, represents a more anorthitic term. The crystallisation of anorthite is compatible with the corresponding calcium content introduced by the SLS glass waste. As regards the other phases detected in the GSTO body, cristobalite was already reported for porcelain stoneware bodies containing waste glass [85,86], whereas clinopyroxene was never previously reported, presumably because of its low amount.

NR and GR were produced from the same raw materials but were fired under different schedules, which resulted in differences in their mineralogical compositions. NR was fired at a relatively low temperature of 820 °C, which led to limited phase reactions. These reactions included the breakdown of calcite and incomplete decomposition of phyllosilicates (illite and mica), which partially transformed into plagioclase and K-feldspar. Quartz and feldspars remained stable under the firing conditions. Thus, most of the crystalline phases were residual, whereas the amorphous/disordered phase mainly resulted from the breakdown of clay minerals. These mineralogical features are consistent with the composition of typical scarcely reacted ceramic bodies, such as certain types of bricks [87,88].

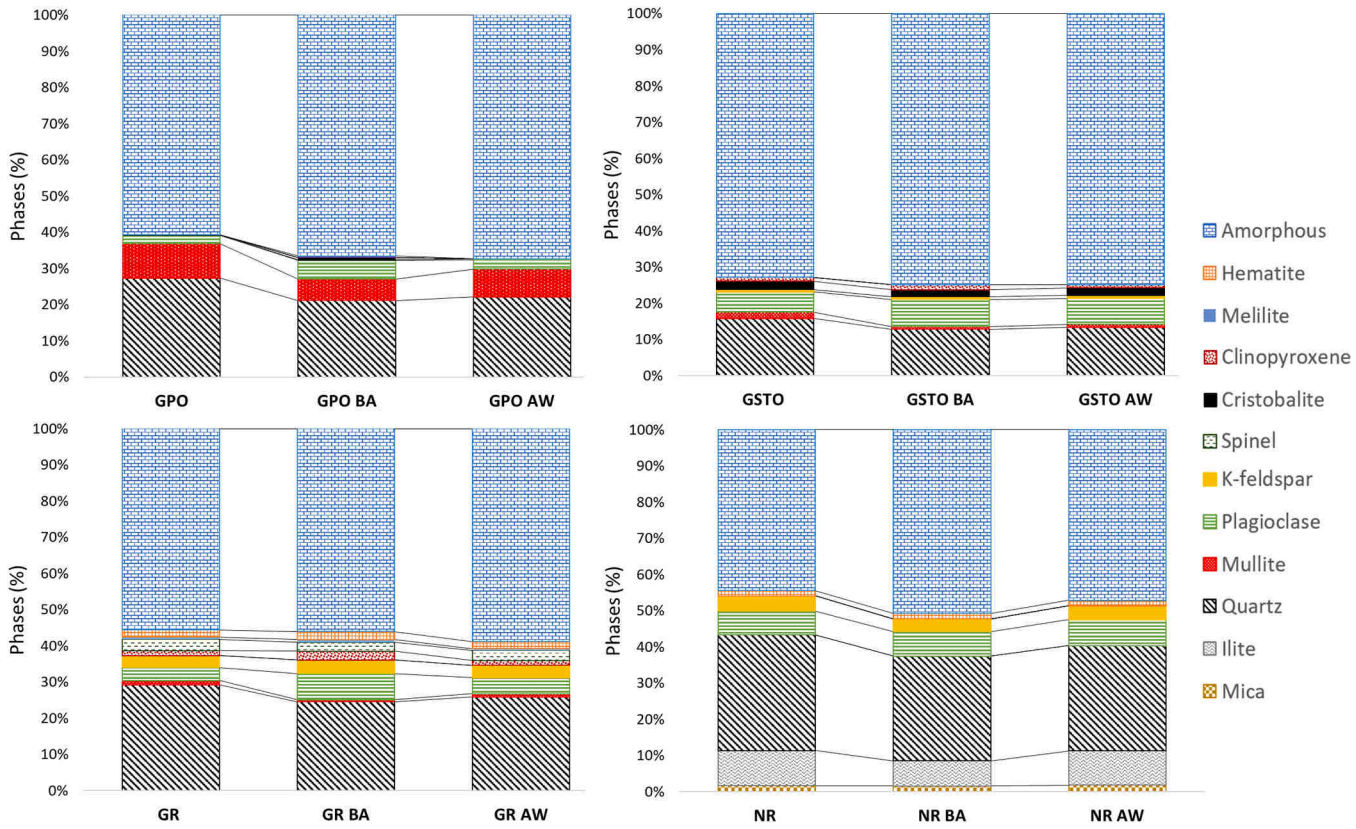

Fig. 1. Phase composition of the fired batches.

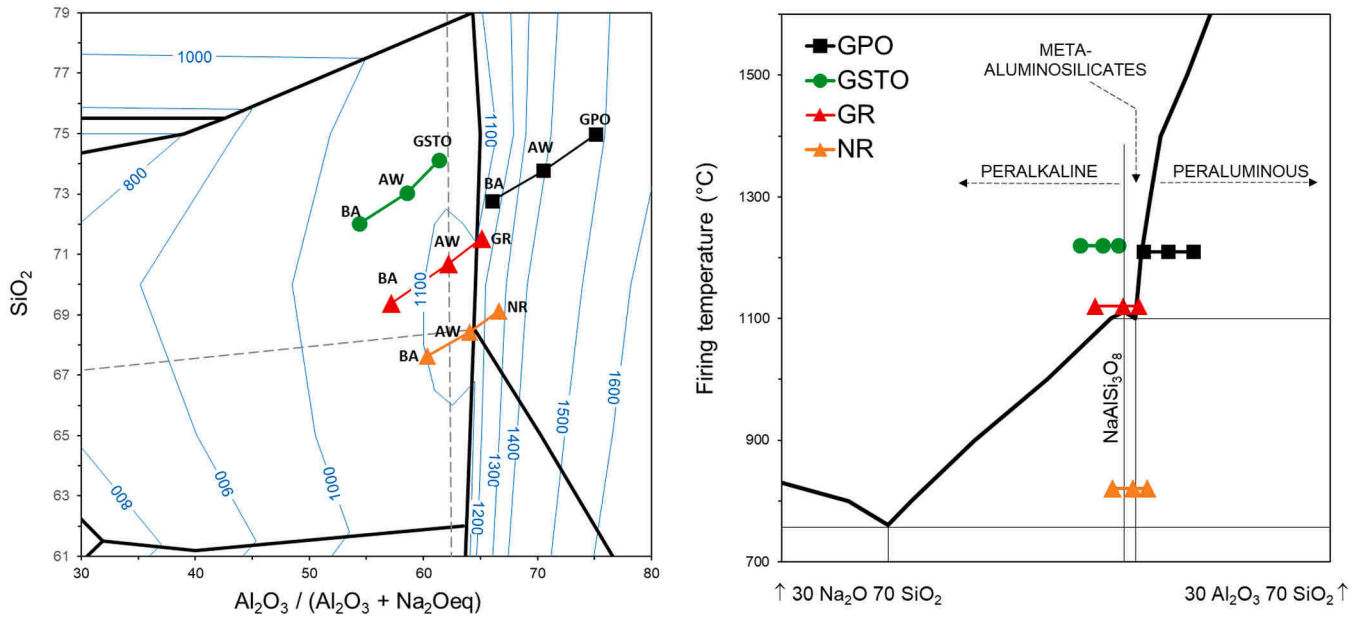

Fig. 2. Chemical compositions of the investigated ceramic bodies in the SiO_2–Al_2O_3–Na_2O ternary phase diagrams (for the diagram construction, see [83]).

The heat treatment of GR at 1120 °C resulted in a complex set of transformations. This process involved the melting of feldspars and illite-mica as well as and the incorporation of amorphous by-products derived from the breakdown of these minerals in a melt, which generates an abundant vitreous phase in the finished product. Furthermore, new crystalline phases such as spinel, melilite, clinopyroxene and mullite formed. Spinel could be a defective structure of the γ-Al_2O_3 phase, likely representing the metastable precursor of mullite [89,90]. Indeed, the considerable presence of its precursor (~3 wt%) would also explain the low content of mullite, justified by the relatively low firing temperature (1120 °C). Melilite formation at low thermal regimes is a common occurrence [87,88]. The presence of clinopyroxene, likely an Al-rich augite solid solution based on the refined unit-cell parameters (Equations 4a to 4d [84]), is consistent with the amounts of Fe_2O_3, MgO and CaO (Table 1). The high vitreous-phase content in the final body classifies the GR batch as a semi-vitrified product.

The samples can be classified based on their technological properties, according to the commercial classification of the ceramic products (ISO 13006 standard). The fired samples confirm that GPO and GSTO, with water absorption < 0.5%, correspond to largely vitrified ceramics (BIa). GR, with water absorption of 6–8%, can be classified as a semi-vitrified product (BIIb), whereas NR, with water absorption ~13%, falls within the field of porous ceramics (BIII) (Table 3).

As regards the impact of waste introduction on phase transformations, it is noteworthy that the addition of 10 wt% of BA or AW resulted in similar trends, with a decrease in quartz and mullite compared with the reference batches. As previously observed for the SLS glass, BA and AW have lower silica content and higher level of alkali and alkaline earth elements than other raw materials. Consequently, their introduction led to ceramic bodies with a peralkaline composition, as shown in Fig. 2. For GPO, which originates from a highly peraluminous body, the waste-containing batches shifted their chemical composition towards the meta-aluminous field. Peralkaline compositions promote the persistence of feldspars, particularly plagioclase, as evidenced by the higher content in the waste-bearing batches. However, such a composition is unfavourable for mullite stability and often detrimental to quartz.

As regards the other neoformation phases, such as cristobalite, clinopyroxene, spinel and melilite, the presence of waste did not cause any substantial variation in their amount. The content of the amorphous phase increased in the presence of waste owing to its fluxing nature. However, the mineralogical observations made so far could not be extended to the NR bodies, which remained a substantially unreacted material even after the waste incorporation.

In-depth mineralogical analyses were crucial to confirm the formation of crystalline/amorphous phases capable of hosting HEs. Many detected phases can accommodate different HEs under specific conditions [6], as discussed in Section 3.3.

3.2. Microstructure and physical features of the ceramic bodies

Figs. 3–5 (and S2–S5, supplementary materials) illustrate the microstructure of the fired bodies as observed through SEM backscattered electrons. The benchmark bodies GPO, GSTO, GR and NR exhibit the typical features of their respective ceramic types (Fig. 3). GPO and GSTO have a compact microstructure with relics of quartz and feldspars, commonly referred to as 'skeleton' of porcelain stoneware. Light-scattering particles, mainly composed of iron, and rounded isolated pores and irregularly shaped pores are also present. The firing process results in the formation of tiny mullite and clinopyroxene crystals, usually a few micrometres in size, which are not clearly visible without etching [82,91]. Crystals and pores are present within an abundant non-crystalline matrix (a viscous phase at high temperature). This matrix promotes the sintering process by wetting the mineral particles and reducing the voids, which increases the bulk density of the ceramic body. The main difference between GPO and GSTO is the porosity, which is reflected in the bulk density (Table 3). GPO is characterised by a lower volume of pores, which are also smaller in size (ranging from a few up to ~20 μm). Contrarily, GSTO exhibits a bimodal pore distribution, with small pores (around 10–20 μm) coexisting with relatively large pores (up to ~70 μm in diameter). This is the effect of 20-wt% SLS glass in the starting batch, which leads to an accelerated vitrification (high content of amorphous phase, Fig. 1) associated with reduced densification efficiency (Table 3). Similar effects have been observed in other batches containing waste or strong fluxes, such as biomass ash [81,92-94], borate-bearing batches [80] and glassy waste in amount > 10 wt% [24,70,75,82,91].

The microstructure of the NR and GR bodies reflects the phase evolution induced by the heat treatment. The low-fired NR batch exhibits characteristics of a porous body with a negligible degree of vitrification. Specifically, it has a 'crystalline' aspect, with sharp-edged crystals predominating. These crystals represent the starting assemblage of the red clay used, composed of quartz, feldspars, calcite and iron oxide grains dispersed in a fine-grained matrix containing clay minerals and porosity. The amorphous phase inferred from XRPD analyses does not represent a vitreous phase obtained by cooling a melt, as in the case of porcelain stoneware, but rather the product of clay minerals breakdown. The high-magnification micrograph shown in Fig. S2 (left) highlights the presence of structural relicts of clay minerals.

Meanwhile, firing the GR body at an increased temperature resulted in a significant loss of angularity of the crystalline grains and to a more compact structure (Fig. 3). This was due to the occurrence of a liquid phase (Fig. S2-right) that reduced porosity and incorporated residual minerals into a vitreous matrix.

The incorporation of waste exerted varying effects on the microstructure of the benchmark bodies, with AW being the most effective,

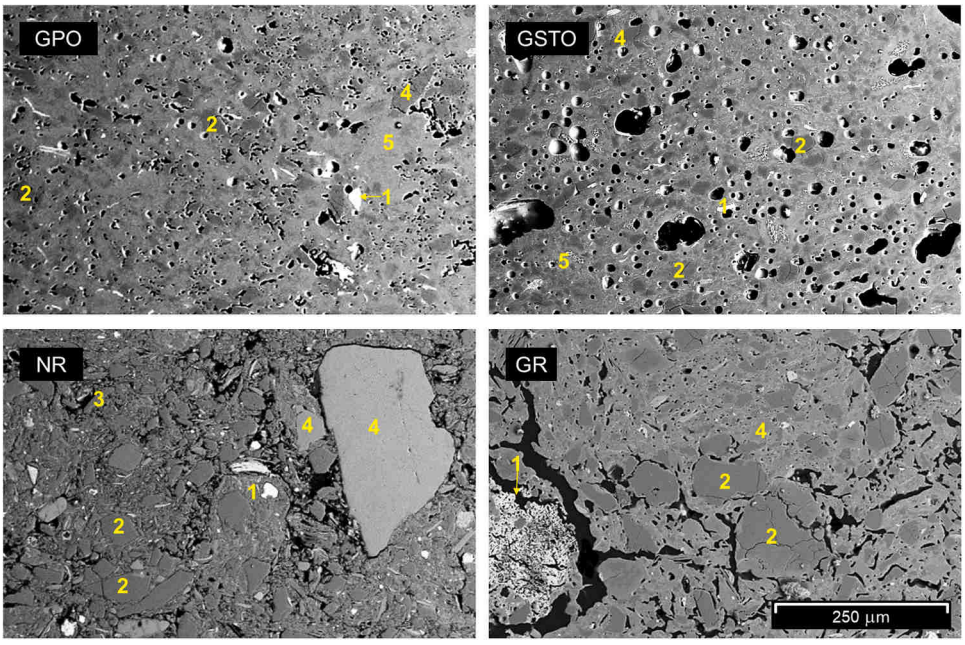

Fig. 3. Microstructure of the benchmark fired bodies: 1 = Fe oxides; 2 = quartz; 3 = clay minerals; 4 = feldspars; 5 = glass.

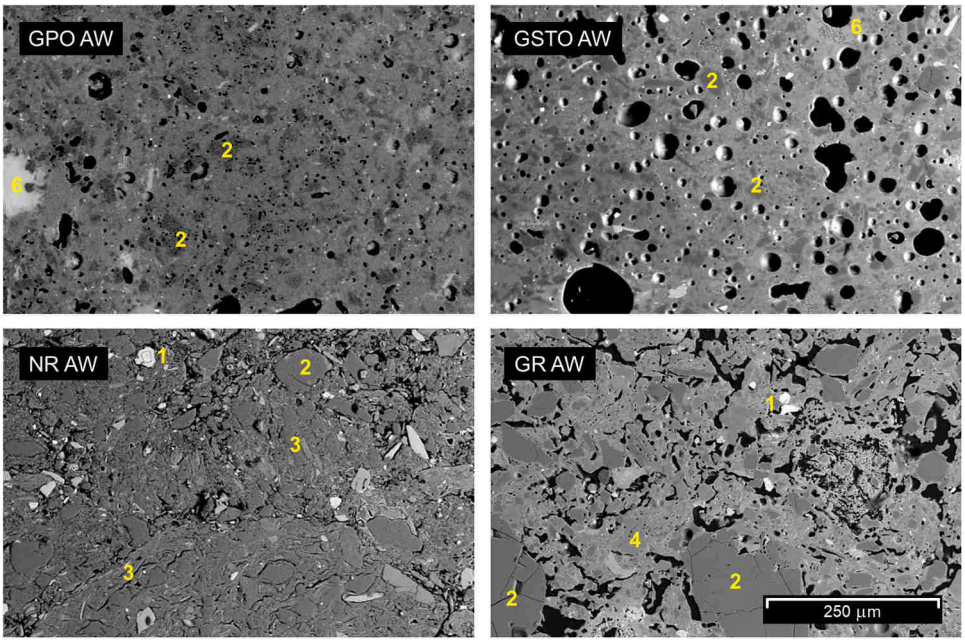

Fig. 4. Microstructure of fired bodies containing artificial waste. 1 = Fe oxides (zircon in GR-AW); 2 = quartz; 3 = clay minerals; 4 = feldspars; 5 = glass; 6 = heavy element diffusion.

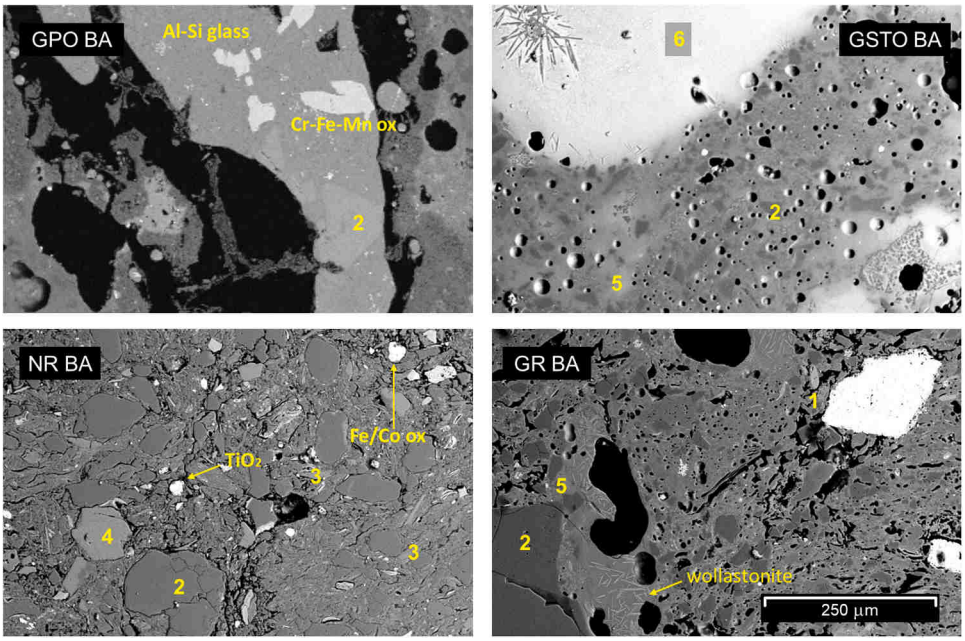

Fig. 5. Microstructure of fired bodies containing bottom ash. 1 = Fe oxides; 2 = quartz; 3 = clay minerals; 4 = feldspars; 5 = glass; 6 = heavy element diffusion.

particularly in GPO and GSTO. Their microstructure (Fig. 4) is not disrupted and can be easily compared with that of the reference bodies (Fig. 3). This suggests a good reactivity of the waste and effective element diffusion. GR and particularly NR are less reacted, so that aggregates of unreacted particles of AW, rich in all the HEs, were sometimes observed.

The case of BA was distinct due to the presence of metallic aggregates (Fe-rich alloys, a known component of BA), which were visible even at a low magnification (Fig. S3, supplementary material). The degree of interaction between the BA and the ceramic bodies appeared to be temperature-dependent, as evidenced by melting and element diffusion during firing. In the largely vitrified bodies, a certain degree of BA melting could be observed. This could lead to the diffusion of heavy elements. However, in GR and NR, there was no considerable exchange between the ceramic matrix and the waste (Fig. 5 and S4-left).

In general, the BA inclusions present in the ceramic matrices exhibited minimal reactivity, even when the ceramic body was fired at high temperatures. These inclusions consist of particles composed of a glassy matrix, HT mineral phases, and metallic or alloy aggregates, which are the same features found in the BA [95]. For instance, a piece of unreacted material from the BA can be observed in GPO (Fig. 5 and S3). The 1-mm fragment consists of an aluminosilicate matrix with Fe-, Cr- and Mn-rich areas (the brighter ones). Rimming this inclusion, a large void is present, which likely resulted from the degassing of

hydrated or carbonate phases during the ceramic process. In GSTO, which was fired at 1220 °C and had the highest melt content at HT favouring the interaction with the BA, partially reacted metallic inclusions are visible (Fig. 5 and S4-right). The diffusion of elements from BA into the ceramic matrix appears to be restricted to the area adjacent to the aggregates, resulting in the dendritic shape typical of BA. These structures are chemically Fe-rich silicates, indicating a high melting temperature and subsequent cooling rates without reaching thermodynamic equilibrium. In the NR ceramic body, BA residues are completely unreacted, with well-defined boundaries and no evidence of element mixing with the ceramic matrix (Fig. S4-left). In the sample GR, we found both unreacted BA particles and elongated neoformation crystals of wollastonite (Fig. 5 and S5, supplementary materials).

Regarding the physical features of the ceramic bodies, the data in Table 3 indicate that the addition of waste did not significantly affect the open porosity, which is determined by water absorption. The only notable change is an increase in porosity in the GR-BA sample, but it still falls under the category of semi-vitrified body. However, highly vitrified samples containing waste exhibit a clear decrease in BD (Table 3). The BD of ceramic products is affected by the total porosity variation. A decrease in BD indicates a higher level of closed porosity, which is actually visible in the SEM micrographs (Figs. 4–5). This phenomenon is caused by the waste, which has a fluxing behaviour [81,83].

It can be concluded that although no particular technological problems have been encountered in the manufacture of ceramic products containing BA, the waste was not completely integrated into the ceramic matrix. The persistence of unreacted grains is likely related to their grain size and the refractoriness of certain components in the BA. As explained in the experimental section, the BA was dry-ground, which may have resulted in the presence of relatively large aggregates that only partially reacted during the short ceramic firing time (~1 h for vitrified materials). Furthermore, despite being composed of ~25-wt% amorphous phase and low-melting minerals (~40 wt%), such as calcite, ettringite and portlandite, certain components of BA, such as melilites and spinels, exhibit high refractoriness [95]. In addition, the substantial heterogeneity of BA makes the prediction of its behaviour extremely challenging.

3.3. Leaching behaviour

The leaching tests were conducted simultaneously in water and in acetic acid solution. The eluates from the former were basic (pH 8–11), whereas those from the latter were acidic (pH 5). The leaching solutions were selected to mimic natural environmental conditions that ceramic materials may undergo during landfilling and to better discriminate the leaching behaviour of HEs. Actually, the reduction of pH resulting from acid rain promotes cation dissolution and may enhance element mobilisation. Acetic acid was selected as it has already been used in the ISO 6486–1 standard for evaluating the leaching of Pb and Cd in ceramic materials. The leaching results for ceramic bodies containing the AW are reported and discussed here.The results of the leaching from the BA-bearing bodies are reported in the supplementary materials (Fig. S6) and must be considered with caution. Microstructural observations suggest that leaching results cannot be solely attributed to the specific incorporation of any of the HEs in the crystalline and/or amorphous phases. This is due to the low degree of interaction between the BA and the ceramic matrices, as previously discussed.

The leaching behaviour was evaluated on the fired bodies, ensuring that the results were not affected by any volatilisation of HEs during the firing process. After applying a correction for loss on ignition, no evidence of volatilisation was observed for Ba, Cu, Pb, Sb and Sn when comparing the concentration in fired bodies with that in unfired bodies. The contents of Co, Cr, Mo, Sr and Zn may experience a slight decrease after firing, so that a minimal volatilisation of HEs cannot be completely ruled out.

3.3.1. Leaching in water and in an acidic environment

To compare the effect of different ceramic matrices on the immobilisation of HEs, the leaching data of the bodies containing the AW are plotted in the binary diagrams in Fig. 6. The elemental concentrations measured in the eluates are listed in Tables S5 and S6 (supplementary materials). Notably, the tests conducted with water as the eluate are affected by the pH increase (Table S5, supplementary materials) caused by metal dissolution. Contrarily, acetic acid maintained a constant pH. The leaching dataset for the GPO-AW and GSTO-AW bodies exhibited similar trends in both basic and acidic environments (Fig. 6 A–B). The extraction of elements generally increased as the pH decreased. Specifically, only acidic solutions mobilised Pb and Co, whereas the extraction of Zn and Cu was enhanced at low pH. The former effect was induced by the formation of $PbCO_3$/$Pb(OH)_2$ and $Co(OH)_2$, which are insoluble in the alkaline solutions achieved in the water-based leaching tests [96,97]. A similar effect can be argued for Zn and Cu, as the formation of insoluble species is expected in alkaline conditions [96-98]. Essentially, GPO-AW exhibited a greater release of Ba (in water), Sr and Co than GSTO-AW. It has been hypothesised that Sr and Ba are more effectively immobilised in GSTO due to the crystallisation of an anorthite-rich phase during firing (Fig. 1 and Table S4). This may be due to the incorporation of Ba [99] and Sr [100,101] at the extra-framework site of the plagioclase crystal structure. In addition, Ba^{2+} and Sr^{2+} may be enriched in the aluminosilicate amorphous phase as charge compensators, enabling Al^{3+} to be part of the tetrahedral glass framework. The higher content of the amorphous phase in GSTO-AW than in GPO-AW is consistent with the more effective immobilisation of Ba and Sr. As regards cobalt, it can be hosted in the clinopyroxene formed in GSTO, which allows for a more efficient retention test [102]. However, Pb and Cu were mobilised to a greater extent in GSTO-AW than in GPO-AW, possibly due to the different glassy phase (Fig. S7), where Cu^{2+} and Pb^{2+} are incorporated with a low oxygen coordination number [103,104]. For the bodies made with the red clay, NR-AW and GR-AW (Fig. 6 C–D), the water and acetic acid solution–based tests exhibited similar trends. This confirmed a higher extraction of all the HEs in the acidic medium, particularly Co–Zn–Pb–Cu, as previously discussed.

In general, the extraction of HEs is more pronounced in NR-AW than in GR-AW. This is particularly evident in the case of Sr, V and Mo, which are completely mobilised in NR-AW in both environments. The distinctive behaviour of NR is attributed to the very low degree of reaction of the ceramic body. In fact, the higher firing temperature of GR enabled the formation of a melt and different crystalline phases able to host HEs, such as clinopyroxene, which can host Cr^{3+}, Cu^{2+}, Zn^{2+} and V^{3+} in octahedral coordination [6]; spinel, which can accommodate Cu^{+}, Zn^{2+} and V^{4+} at its tetrahedral site; and Cu^{2+}, Zn^{2+}, Cr^{3+} and V^{3+} at its octahedral site [6,105,106].

Fig. 6 (E to H) presents a comparison of the two porcelain stoneware and the red stoneware. With respect to GPO-AW and GSTO-AW, there was a greater release of all HEs for GR-AW. The exceptions were Zn and Cu in water at very low concentrations (elements that could be accommodated in clinopyroxene and/or spinel of GR-AW) and Ba at acid pH (possibly hosted in melilite). The generally lower retention of GR-AW appears to be at odds with the considerable occurrence of neoformation crystalline phases capable of hosting HEs, as previously described. One potential explanation for this discrepancy is the different compositions of the glassy phase, which is more depolymerised in the GR bodies (see NBO/T parameter in Table S7, supplementary materials). However, the grain size of the leached samples must also be considered. The EN 12457–2:2002 standard for the leaching test specifies samples with a grain size < 4 mm but does not provide any indication of the grain-size distribution. All fired bodies were treated in the same manner (dry-crushing using a hammer) to obtain suitable samples for leaching. However, due to the more compact structure of porcelain stoneware, it was more challenging to crush the material, which resulted in a coarser grain-size distribution than that of the red stoneware, which had a significant fine fraction (see experimental section). A finer grain-size